Journal of Hazardous Materials 179 (2010) 559–563

Contents lists available at ScienceDirect

Journal of Hazardous Materials

journal homepage: www.elsevier.com/locate/jhazmat

Hydrothermal removal of Sr^{2+} in aqueous solution *via* formation of Sr-substituted hydroxyapatite

Sheng-Heng Tan, Xue-Gang Chen, Ying Ye*, Jie Sun, Ling-Qing Dai, Qian Ding

Department of Ocean Science and Engineering, Zhejiang University, Hangzhou 310028, People's Republic of China

ARTICLE INFO

Article history:
Received 7 September 2009
Received in revised form 12 February 2010
Accepted 8 March 2010
Available online 15 March 2010

Keywords:
Hydroxyapatite
Sr removal
Precipitation
Hydrothermal treatment
High level waste (HLW)

ABSTRACT

We removed Sr^{2+} in simulating wastewater and simultaneously prepared Sr-substituted hydroxyapatite *via* chemical precipitation and hydrothermal treatment. Both higher initial pH value and higher molar ratio of Sr/(Sr + Ca) contributed to lower residual Sr^{2+} concentration and higher removal efficiency. About two thirds of Sr^{2+} residual in solution after chemical precipitation were further reduced by hydrothermal treatment. The optimal Sr removal result was 99.66% with an ultimate concentration of 2.0 mg L^{-1} when the initial pH was 12 and Sr/(Sr + Ca) was 0.2. Sr-substituted hydroxyapatite phase with hexagonal structure was identified by XRD and EDS results. However, it was found that $SrHPO_4$ phase was formed in the samples with high Sr composition. The lattice constants became larger with the increase of Sr^{2+} and the crystallinity became higher with the increase of pH value. Rod-like particles were observed in SEM images of synthesized Sr-substituted hydroxyapatite samples, with the size of 20–30 nm in width and 70–100 nm in length. With little secondary waste and simple treating procedure, this method is an effective and prospective measure to deal with ^{90}Sr in nuclear waste and industry wastewater.

1. Introduction

Radiostrontium (^{90}Sr and ^{89}Sr), a contaminant produced in the nuclear fission of ^{235}U and ^{239}Pu [1], is generally found in the high level waste (HLW) of nuclear reaction or groundwater [2,3]. Because ^{90}Sr has persistent radioactivity and biological toxicity, and long half-life of 28.9 years, it should be removed from HLW to protect humanity and environment [4]. Moreover, its lasting exothermicity makes it harmful to immobilize the radioactive waste by vitrification in final geological disposal [5]. Therefore, the removal of radiostrontium from HLW has attracted numerous attentions in recent years.

Currently, there are many methods to treat ^{90}Sr in the HLW, among which separation by liquid–liquid solvent organic extraction using special derivatives of crown ethers is in mainly use [6,7]. These derivatives have shown excellent capability and particular selectivity for Sr^{2+} than other cations. More than 90% ^{90}Sr dissolved in nitric acid can be separated by the adsorption of crown ether in porous carrier [8]. However, this method usually generates a lot of secondary organic waste and it can only separate the Sr^{2+} from waste but cannot preserve it for long-term conservation. Meanwhile, other methods [9–12] are reported such as adsorption by activated carbon, maize tassel and moss, with a large scale removal of from 74% to 98%. The deficiency of these methods is lack of repeatability, for their materials are mainly natural substances that are narrowly distributed. Precipitation, which could remove the Sr^{2+} in the waste by chemical reaction, is used to immobilize hazardous ions into precipitate, and if the precipitate could provide a long-term preservation for such ions, this method will be promising to purify waste. Our group is trying not only to immobilize $^{90}Sr^{2+}$ ions into solid products but also to simultaneously and directly form a kind of matter that could conserve them for a long time.

Hydroxyapatite, with a low solubility of 5.4×10^{-119} (K_{sp}, $mol^{18}\,L^{-18}$, neutral pH solution) [13], is considered to be an ideal material to precipitate Sr^{2+} in liquid solution [14]. The two different Ca^{2+} sites in the hydroxyapatite structure can be easily substituted by other metal cations, especially the divalent cations [15–17]. Thus it is available for Sr^{2+} to incorporate into the hydroxyapatite structure. Also, hydroxyapatite can be tailored to be a porous structure [18,19], which makes it possible to further adsorb Sr^{2+} in solution. Furthermore, hydroxyapatite shows high adsorptive capability for heavy elements such as actinides and lanthanides [15,20], rapid recovery capability after being irradiated [21] and excellent thermal and chemical stability under various conditions [22,23], indicating that it can be used for the long-term preservation of radio elements. Sintered hydroxyapatite with other minerals has been studied for the treatment of radioactive elements in nuclear waste in Japan [13], but few reports mention to directly incorporate Sr^{2+} into hydroxyapatite structure during its formation. Additionally, hydroxyapatite can also be used to remove toxic heavy metal ions in indus-

* Corresponding author. Tel.: +86 571 87953217; fax: +86 571 87951411/336.
E-mail address: tanshengheng@zju.edu.cn (Y. Ye).

0304-3894/$ – see front matter © 2010 Elsevier B.V. All rights reserved.
doi:10.1016/j.jhazmat.2010.03.040

trial waste due to its high adsorptive and substituent capability [14].

Hydroxyapatite can be produced by various methods such as hydrothermal method [24,25], sol–gel method [26], chemical precipitation [27] and other methods. In this study, we removed Sr^{2+} in the simulating HLW and afterwards prepared Sr-substituted hydroxyapatite ($Sr_xCa_{10-x}(PO_4)_6(OH)_2$) *via* chemical precipitation and hydrothermal treatment. Hydrothermal treatment was used to promote the extent of precipitation and adsorption. Sodium tri-polyphosphate (STPP) was introduced in the synthetic and hydrothermal process, because it is reported that STPP could catalyze the synthesis of hydroxyapatite [28] and enhance the dispersive properties of products [29]. More than 99% Sr^{2+} in simulating solution was immobilized to solid products and pure Sr-substituted hydroxyapatite phase was identified. In addition, we investigated the influence factors such as initial pH values and initial Sr concentrations on the removal efficiency of Sr^{2+}.

2. Experimental

2.1. Materials

$Ca(NO_3)_2{\cdot}4H_2O$ (236.15, AR) and $Sr(NO_3)_2$ (211.63, AR) were purchased from Sinopharm Chemical Reagent Co. Ltd. (Shanghai, China). Na_2HPO_4 (141.98, AR) and NaOH (40.01, AR) were supplied by Huzhou Chemical Reagent Factory (Huzhou, China). Sodium tripolyphosphate (STPP, $Na_5P_3O_{10}$, 367.86, AR) was obtained from Wenzhou Dongsheng Chemical Reagent Factory (Wenzhou, China).

2.2. Removal of Sr^{2+} and formation of Sr-substituted hydroxyapatite

2.2.1. Precipitation

A mixed metal nitrate solution (0.1 mol L^{-1} for metal ions) was prepared from $Ca(NO_3)_2{\cdot}4H_2O$ and $Sr(NO_3)_2$, in which the molar ratio of Sr/(Sr + Ca) varies from 0.1 to 1. Na_2HPO_4 was dissolved in deionized water to reach a 0.06 mol L^{-1} solution, the pH of which was adjusted to 10 or 12 by 0.5 mol L^{-1} NaOH solution. The metal nitrate solution (50 mL) was then dropwise added into 50 mL Na_2HPO_4 solution under continuous stirring at 50 °C.

2.2.2. Hydrothermal treatment

Then, STPP solution (50 mL, 20 g L^{-1}) was introduced into the reaction solution and continued stirring for 0.5 h. 80 mL homogeneous mixture of precipitation and solution was poured into a 100 mL Teflon-lined stainless autoclave, heated at 160 °C for 14 h hydrothermal condition.

After centrifugation, the clear liquid solution in autoclave was used to determine the residual strontium concentration and the solid product was collected after washing with deionized water and drying at 80 °C for 12 h. Then, the dried product was prepared for the characterization of XRD, SEM and EDS. According to the initial molar ratio (r) of Sr/(Ca + Sr) (0.1, 0.2, 0.3, 0.4, 1) and pH value of Na_2HPO_4 solutions (10, 12), the samples were named as 100*r*SrHA-pH.

2.3. Characterization of samples

The concentrations of Sr^{2+} were measured by atomic adsorption spectroscopy (AAS, Hitachi180-50, Japan). The dried samples were characterized by X-Ray diffraction (XRD, D/max-IIB, Japan) with Cu Kα radiation (40 kV and 100 mA). XRD data used for structural analysis were collected by step scanning method under the 2θ range 3–80°, step width of 0.2° and counting time 6 s. The morphologies of synthesized products were observed by an S-4800 scanning electronic microscope (SEM, Hitachi, Japan and Ultro 55, Germany). Chemical composition of products was determined by energy dispersive spectroscopy (EDS, EDS7426, Britain).

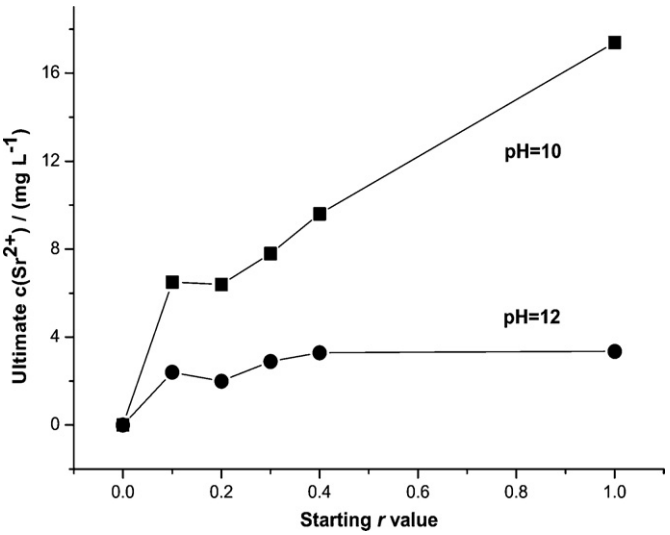

Fig. 1. Effect of initial pH and r on the residual Sr^{2+} concentration in solution.

3. Result and discussion

3.1. Removal efficiency of Sr^{2+}

The following chemical equation is the principle of removal reaction:

$$xCa^{2+} + (10-x)Sr^{2+} + 6HPO_4{}^{2-} + 8OH^- \rightarrow Ca_xSr_{10-x}(PO_4)_6(OH)_2 \downarrow + 6H_2O \quad (1)$$

Under the alkaline condition, Sr^{2+} and Ca^{2+} were precipitated by $HPO_4{}^{2-}$ to Sr-substituted hydroxyapatite. The liquid samples (each of 5 mL) were abstracted from the clear solution before and after hydrothermal and diluted to 100 mL, respectively.

3.1.1. Influence of initial pH and r values

Figs. 1 and 2 show the variation between the ultimate removal of Sr^{2+} (after precipitation and hydrothermal treatment) and initial pH in Na_2HPO_4 solution, or initial r values. As seen in Fig. 1, the

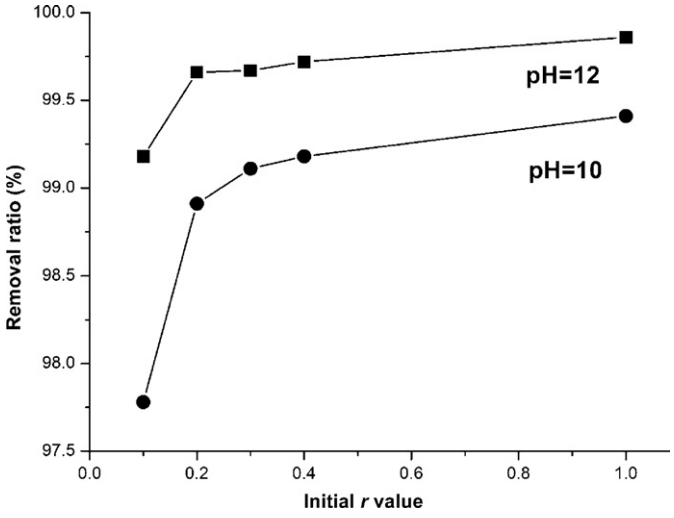

Fig. 2. Effect of initial pH and r on the removal ratio.

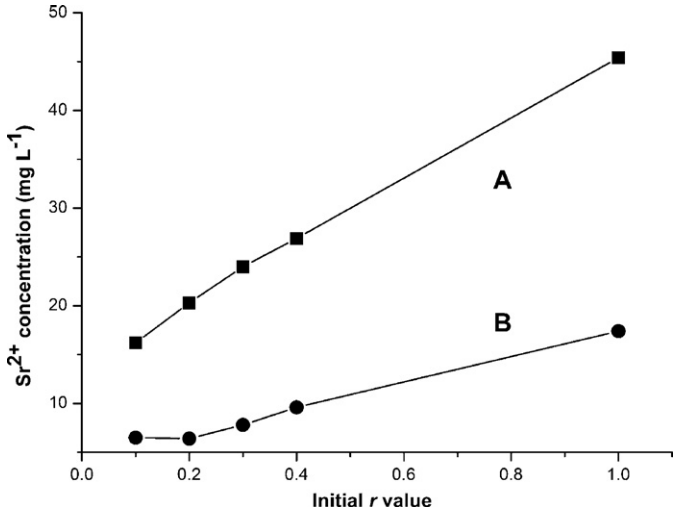

Fig. 3. Effect of hydrothermal treatment on Sr^{2+} concentration at initial pH of 10. A and B respectively represent the Sr^{2+} concentration before and after the hydrothermal treatment.

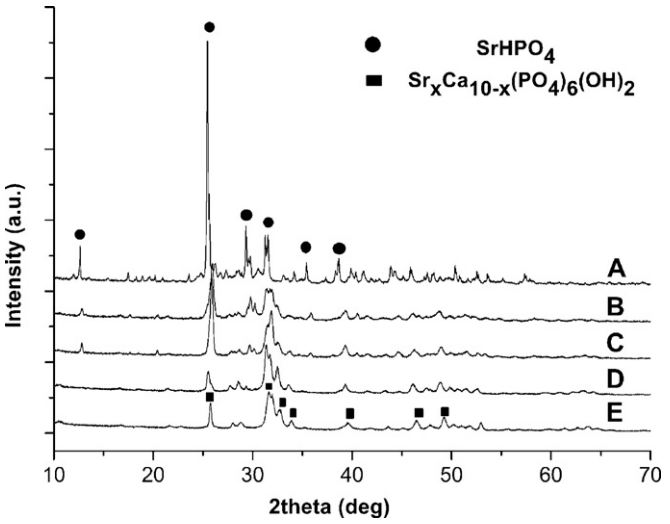

Fig. 4. XRD patterns of samples (pH 12) under different initial *r* values: (A) 1, (B) 0.4, (C) 0.3, (D) 0.2, (E) 0.1.

removal result of Sr^{2+} is highly pH dependent as well as initial *r* values dependent. The increase of pH value contributed to a marked decrease of residual Sr^{2+} concentration (from 6.4 mg L^{-1} at pH of 10 to 2 mg L^{-1} at pH of 12, at $r = 0.2$) and the increase of removal ratio (from 99.11% to 99.67% at $r = 0.3$). Meanwhile, the residual Sr^{2+} concentration increased slightly with *r* values at pH of 12 while it went up dramatically when pH turned to 10. Both at pH of 10 and 12, the lowest Sr^{2+} concentration appeared at $r = 0.2$, not the lowest initial *r* of 0.1, though their figures were quite approximate. The results suggest that the ultimate Sr^{2+} concentration will not unlimitedly decrease with the decline of initial *r* value, but maintain at an approximately constant level or even slightly increase at low-*r*-value samples. The removal ratio of Sr^{2+} in both pH groups increased gradually, approaching to an ultimate figure of 99.41% (pH 10) and 99.86% (pH 12), respectively.

The significant influence of pH to the removal results can be attributed to two reasons. First, hydroxyapatite is an alkalescent substance. Higher pH value in initial Na_2HPO_4 solution can not only provide the reaction with a more beneficial circumstance to form precipitate but also promote the extent of reaction, which will incorporate more metal irons into solid phase. Second, hydrothermal treatment is sensitive to pH value. During the hydrothermal process, higher pH value will accelerate the re-precipitation and enhance the adsorption of Sr^{2+} in solution. Meanwhile, the close concentrations of 10SrHA and 20SrHA can be explained by the concentration limit of Sr^{2+} in this system, because of the chemical balance between the formation of Sr-substituted hydroxyapatite and Sr^{2+} in solution.

In summary, the residual concentration and removal ratio simultaneously increased with *r* and higher pH improved the removal results. The main aim of our study is to attain lowest residual concentration and highest removal ratio, thus the optimal experimental condition was at pH of 12 and *r* of 0.2, with 99.66% of Sr removed and an ultimate concentration of 2.0 mg L^{-1}.

3.1.2. Effects of precipitation process and hydrothermal treatment

According to Fig. 3, the Sr^{2+} was primarily removed by the precipitation process, however still leaving a high level ranging from 16.2 mg L^{-1} ($r = 0.1$) to 45.2 ($r = 1$) mg L^{-1}. Then, the Sr^{2+} concentration further decreased by around two thirds to the ultimate concentration from 6.4 to 17.4 mg L^{-1} after hydrothermal treatment at 160 °C for 14 h. The Sr^{2+} concentration increased linearly and steadily with *r* value before hydrothermal treatment, whereas, the upward trend turned to much slighter after hydrothermal treatment. Hydrothermal treatment improved removal results, by promoting the re-crystallization of solid products and further adsorption of Sr^{2+}. Thus, hydrothermal condition is necessary in our study to achieve better removal effect.

3.2. Synthesis of Sr-substituted hydroxyapatite

3.2.1. Effect of initial r

As can be seen in Fig. 4, only hexagonal Sr-substituted hydroxyapatite (34-0480 to 34-0484) can be identified in the XRD patterns of 20SrHA-12 and 10SrHA-12, according to the two highest peaks at 2θ angles of around 31.6° and 33.8° which represent (2 1 1) and (3 0 0) plane, respectively. However, not only Sr-substituted hydroxyapatite but also $SrHPO_4$ phase (33-1335, characterized by diffraction peaks of (−1 0 2), (2 0 0) and (0 0 1) planes at around 25.4°, 25.6° and 12.6°, respectively) was identified in both 40SrHA-12 and 30SrHA-12, and finally only pure $SrHPO_4$ phase with triclinic structure was identified in 100SrHA-12.

EDS results in Table 1 also indicate the immobilization of Sr to solid products and the emergence of $SrHPO_4$ with the increase of initial *r*. While the Sr/Ca molar ratio in sample 10SrHA-12 and 20SrHA-12 is very close to the initial *r* values, in higher-*r* samples it differs distinctly from the expected ratio. Meanwhile, the (Sr + Ca)/P molar ratio results have shown similar changes in compositions. This ratio in samples 10SrHA-12 and 20SrHA-12 is 1.68 and 1.62, respectively. However, it plunges sharply in other samples, and finally declines to only 1.06. These results are also accordant to the XRD results: lower-*r* samples are primarily made up of Sr-substituted hydroxyapatite, so the (Ca + Sr)/P molar ratio of them is around 1.67, the stoichiometric Ca/P ratio of hydroxyapatite [$Ca_{10}(PO_4)_6(OH)_2$]. Higher-*r* samples contain increasingly strontium mono-phosphate ($SrHPO_4$) with the increase of initial *r*,

Table 1
Atomic ratio of Sr, Ca and P in samples.

Sample	Ca (%)	Sr (%)	Ca:Sr	Expected Ca:Sr	P (%)	(Sr + Ca)/P
10SrHA-12	23.52	2.62	8.98	9	15.59	1.68
20SrHA-12	19.81	5.08	3.90	4	15.09	1.65
30SrHA-12	16.26	8.80	1.85	2.33	16.08	1.56
40SrHA-12	13.13	11.84	1.11	1.5	16.92	1.48
100SrHA-12	0	16.28	–	–	15.43	1.06

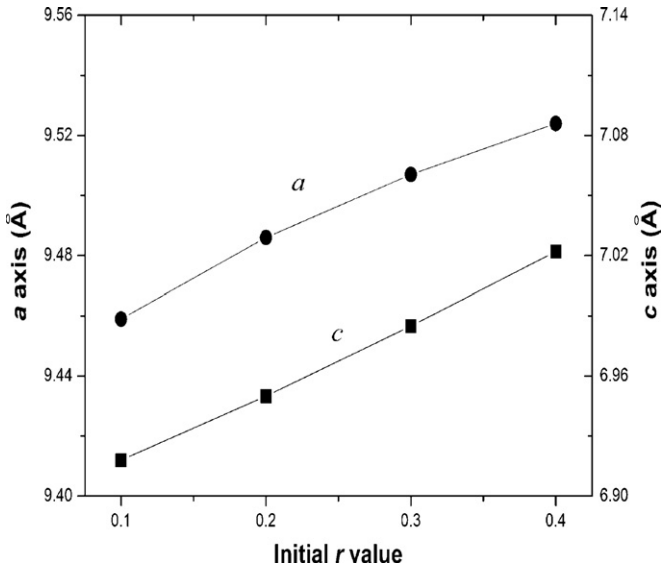

Fig. 5. Lattice constants of solid products (pH 12) against r value.

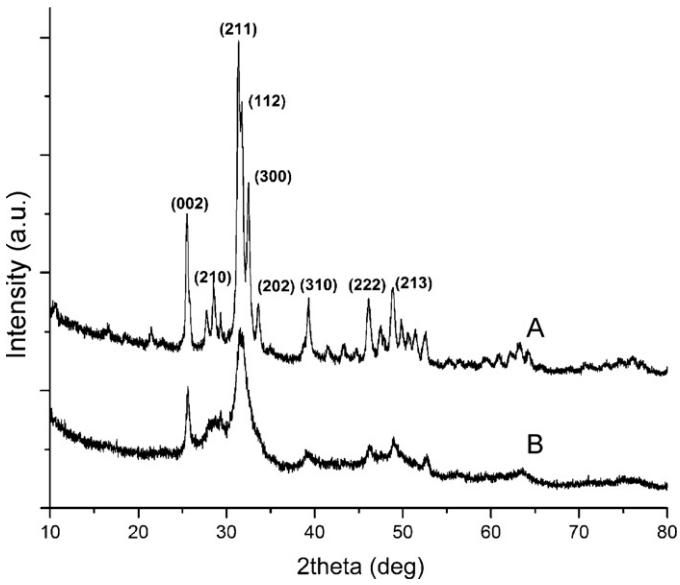

Fig. 6. XRD patterns of samples (r = 0.2) in different pH values: (A) pH 12, (B) pH 10.

making this ratio gradually decrease to 1, the stoichiometric ratio of $SrHPO_4$.

The emergence of $SrHPO_4$ observed in products is related to the increase in supersaturation to incorporate Sr^{2+} into hydroxyapatite structure with the rise of r value. Furthermore, conditions are not enough to form Sr hydroxyapatite so that the surplus Sr is precipitated as $SrHPO_4$. Biphosphate is prone to be dehydrated to form pyrophosphate or metaphosphate [30], thus $SrHPO_4$ is not suitable in our study for conserving Sr^{2+}. Therefore, the r value should be controlled at a low level to form products mainly in hydroxyapatite structure.

A slight shift to lower 2θ angles of Sr-substituted hydroxyapatite peaks with the increase of r was observed in Fig. 4, indicating that parts of Ca^{2+} site in hydroxyapatite was successfully replaced by Sr^{2+}. Ion radius of Sr is larger than that of Ca (1.13 Å of Sr^{2+} against 0.99 Å of Ca^{2+}, in 6-coordinate octahedral site) [31], thus the incorporation of Sr contributed to larger crystal lattice, as shown in Fig. 5. In hexagonal structure, a and c became linearly larger with r values, indicating that the Sr-substituted hydroxyapatite solid solutions were continuous solid solutions in the range of 0.1–0.4. Therefore, synthesized Sr-substituted hydroxyapatite can be tailored to be with various Sr compositions.

3.2.2. *Effect of initial pH in Na_2HPO_4 solution*

As shown in Fig. 6, both A (for 20SrHA-12) and B (for 20SrHA-10) were identified to be $Ca_xSr_{10-x}(PO_4)_6(OH)_2$ solid solution phase with x of 8,which was in accordance with the initial ratio. However, A exhibited much higher intensity and lower half peak width than those of B. Moreover, the main peaks of (2 1 1), (1 1 2) and (3 0 0)

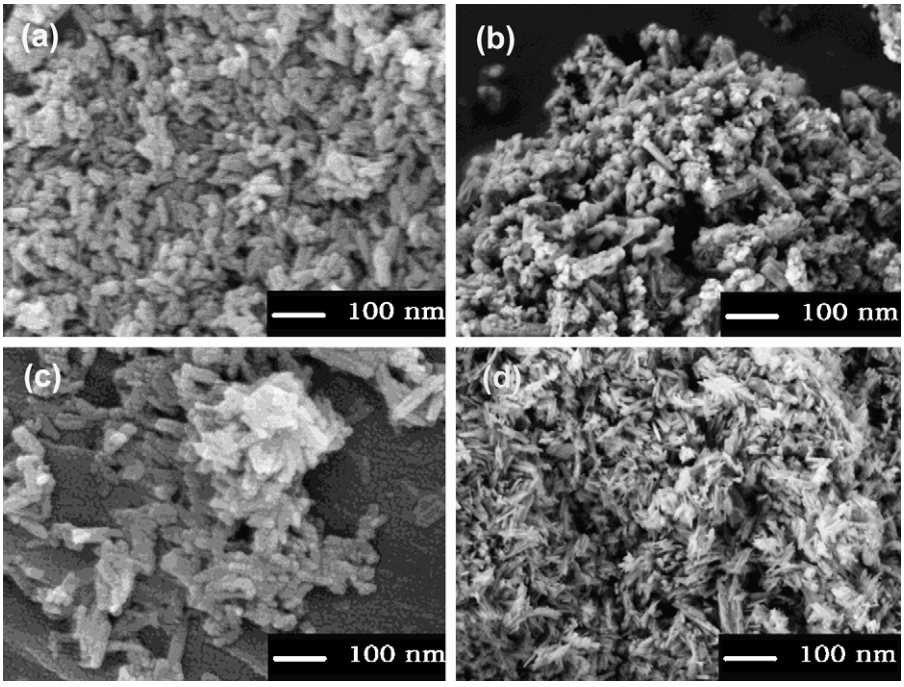

Fig. 7. SEM image of samples (pH 12): (a) r = 0.1, (b) r = 0.2, (c) r = 0.3, (d) r = 1.

between 31.3° and 32.5° were much more evident in A, while those peaks were hard to be identified in B. These differences indicated that A samples had a higher crystallinity degree which was beneficial to achieve a higher extent of reaction and to immobilize more Sr^{2+} into precipitate.

The increase of crystallinity degree with pH can be attributed to the contribution of pH to precipitation and hydrothermal process. Higher pH in initial solution provided a more instructive environment to form Sr-substituted hydroxyapatite and avoid the emergence of amorphous substance. In hydrothermal process, higher pH value led the re-dissolution and re-crystallization to the direction that formed higher crystallized products.

3.3. SEM results

Fig. 7 shows SEM photographs of the products prepared by hydrothermal treatment with different *r* values. It can be observed that rod-like crystals were dominant in Fig. 7a–c ($r = 0.1–0.3$), but only stinging particles in Fig. 7d ($r = 1$). While most of the particles in Fig. 7a and b were dispersed homogeneously and densely, the particles in Fig. 7c were mainly aggregated to bulks and dispersed incompactly. Moreover, although no aggregation can be found in Fig. 7d, the morphology of particles has changed, indicating that there was mainly another kind of matters in the products. The size of the crystals increased with the *r* value, from an average of 20 nm in width and 70 nm in length (Fig. 7a) to 30 nm in width and 100 nm in length (Fig. 7c).

The introduction of $SrHPO_4$ contributed to the alteration in particle distribution and its morphology. In the re-crystallization of hydrothermal process, the emergence of $SrHPO_4$ led to heterogeneous nucleation in solution, which caused the unbalanced growth and agglomeration in Fig. 7c. Smaller size and uniform distribution of particles are more beneficial for the later sintering treatment, which will make the sintered ceramic more densified and homogeneous.

4. Conclusions

In summary, Sr^{2+} was substantially removed (an optimal result of 99.7% removal with the ultimate concentration of 2.0 mg L^{-1}) from the solution and the Sr-substituted hydroxyapatite was successfully synthesized by chemical precipitation and hydrothermal treatment. The initial *r* value and pH in Na_2HPO_4 have great influence on the removal of Sr^{2+} and formation of Sr-substituted hydroxyapatite. Hydrothermal treatment can promote the removal effect by further precipitation and sorption. While rod-like particles were predominant in low-*r*-value samples, stinging and agglomerated particles were found in high-*r*-value samples. This method is promising to be an effective way to remove and immobilize the $^{90}Sr^{2+}$ in nuclear waste and Sr^{2+} in industry waste. Besides the high removal efficiency and nonpolluting treatment process, the Sr-substituted hydroxyapatite we synthesized can be used for geological conservation of ^{90}Sr because of its outstanding capability for accommodating radioactive elements.

However, some problems are still needed to be solved in our study, such as the properties of the samples after sintering, how to reduce the introduction of $SrHPO_4$ and the influence of particle morphologies on the removal effect. These problems are involved in our recent work and we will continue ameliorating the method to remove Sr^{2+}.

References

[1] M.J. O'Hara, S.R. Burge, J.W. Grate, Automated radioanalytical system for the determination of Sr-90 in environmental water samples by Y-90 Cherenkov radiation counting, Anal. Chem. 81 (2009) 1228–1237.

[2] G.E. Gurboga, H. Tel, Preparation of TiO_2-SiO_2 mixed gel spheres for strontium adsorption, J. Hazard. Mater. 120 (2005) 135–142.

[3] T.C. Chu, J.J. Wang, Y.M. Lin, Radiostrontium analytical method using crown-ether compound and Cerenkov counting and its applications in environmental monitoring, Appl. Radiat. Isotopes 49 (1998) 1671–1675.

[4] A. Nilchi, M.R. Hadjmohammadi, S.R. Garmarodi, Studies on the adsorption behavior of trace amounts of $^{90}Sr^{2+}$, $^{140}La^{3+}$, $^{60}Co^{2+}$, Ni^{2+} and Zr^{4+} cations on synthesized inorganic ion exchangers, J. Hazard. Mater. 167 (2009) 531–535.

[5] A.Y. Zhang, W.H. Wang, Z.F. Chai, Separation of strontium ions from a simulated highly active liquid waste using a composite of silica-crown ether in a polymer, J. Sep. Sci. 31 (2008) 3148–3155.

[6] A.Y. Zhang, W.H. Wang, Z.F. Chai, Modification of a novel macroporous silica-based crown ether impregnated polymeric composite with 1-dodecanol and its adsorption for some fission and non-fission products contained in high level liquid waste, Eur. Polym. J. 44 (2008) 3899–3907.

[7] B.J. Howard, N. Semioschkina, G. Voigt, Radiostrontium contamination of soil and vegetation within the Semipalatinsk test site, Radiat. Environ. Biophys. 43 (2004) 285–292.

[8] T.L. Yost, B.C. Fagan, L.R. Allain, Crown ether-doped sol–gel materials for strontium (II) separation, Anal. Chem. 72 (2000) 5516–5519.

[9] M. Krishna, S.V. Rao, J. Arunachalam, Removal of Cs-137 and Sr-90 from actual low level radioactive waste solutions using moss as a phyto-sorbent, Sep. Purif. Technol. 38 (2004) 149–161.

[10] S. Chegrouche, A. Mellah, A. Barkat, Removal of strontium from aqueous solutions by adsorption onto activated carbon: kinetic and thermodynamic studies, Desalination 235 (2009) 306–318.

[11] T. Kikuchi, I. Goto, K. Suzuki, Separation of actinoids from HLW by thiacalix[4]arene compound impregnated silica ion-exchanger, Prog. Nucl. Energ. 47 (2005) 397–405.

[12] C.M. Zvinowanda, J.O. Okonkwo, M.M. Sekhula, Application of maize tassel for the removal of Pb, Se, Sr, U and V from borehole water contaminated with mine wastewater in the presence of alkaline metals, J. Hazard. Mater. 164 (2009) 884–891.

[13] Y. Watanabe, T. Ikoma, Y. Suetsugu, The densification of zeolite/apatite composites using a pulse electric current sintering method: a long-term assurance material for the disposal of radioactive waste, J. Eur. Ceram. Soc. 26 (2006) 481–486.

[14] K.J. Zhu, K. Yanagisawa, A. Onda, Hydrothermal synthesis and morphology variation of cadmium hydroxyapatite, J. Solid State Chem. 177 (2004) 4379–4385.

[15] P. Martin, G. Carlot, A. Chevarier, Mechanisms involved in thermal diffusion of rare earth elements in apatite, J. Nucl. Mater. 275 (1999) 268–276.

[16] K.J. Zhu, K. Yanagisawa, R. Shimanouchi, Synthesis and crystallographic study of Pb-Sr hydroxyapatite solid solutions by high temperature mixing method under hydrothermal conditions, Mater. Res. Bull. 44 (2009) 1392–1396.

[17] I. Smiciklas, S. Dimovic, I. Plecas, Removal of Co^{2+} from aqueous solutions by hydroxyapatite, Water Res. 40 (2006) 2267–2274.

[18] U. Ripamonti, Osteoinduction in porous hydroxyapatite implanted in heterotopic sites of different animal models, Biomaterials 17 (1996) 31–35.

[19] Y.H. Kim, H. Song, D.H. Riu, Preparation of porous Si-incorporated hydroxyapatite, Curr. Appl. Phys. 5 (2005) 538–541.

[20] F.G. Simon, V. Biermann, B. Peplinski, Uranium removal from groundwater using hydroxyapatite, Appl. Geochem. 23 (2008) 2137–2145.

[21] H. Sato, B.A. Filas, S.S. Eaton, Electron spin relaxation of radicals in irradiated tooth enamel and synthetic hydroxyapatite, Radiat. Meas. 42 (2007) 997–1004.

[22] N.Y. Mostafa, Characterization, thermal stability and sintering of hydroxyapatite powders prepared by different routes, Mater. Chem. Phys. 94 (2005) 333–341.

[23] I. Cacciotti, A. Bianco, M. Lombardi, Mg-substituted hydroxyapatite nanopowders: synthesis, thermal stability and sintering behaviour, J. Eur. Ceram. Soc. 29 (2009) 2969–2978.

[24] P. Parhi, A. Ramanan, A.R. Ray, Hydrothermal synthesis of nanocrystalline powders of alkaline-earth hydroxyapatites, $A_{10}(PO_4)_6(OH)_2$, J. Mater. Sci. (2006) 1455–1458.

[25] V. Jokanovic, D. Izvonar, M.D. Dramicanin, Hydrothermal synthesis and nanostructure of carbonated calcium hydroxyapatite, J. Mater. Sci.: Mater. Method (2006) 539–546.

[26] A.H. Rajabi-Zamani, A. Behnamghader, A. Kazemzadeh, Synthesis of nanocrystalline carbonated hydroxyapatite powder via nonalkoxide sol–gel method, Mater. Sci. Eng. C 28 (2008) 1326–1329.

[27] I. Mobasherpour, M.S. Heshajin, A. Kazemzadeh, Synthesis of nanocrystalline hydroxyapatite by using precipitation method, J. Alloy Compd. 430 (2007) 330–333.

[28] H.B. Zhang, K.C. Zhou, Z.Y. Li, Plate-like hydroxyapatite nanoparticles synthesized by the hydrothermal method, J. Phys. Chem. Solids 70 (2009) 243–248.

[29] A. Papo, L. Piani, R. Ricceri, Sodium tripolyphosphate and polyphosphate as dispersing agent for kaolin suspensions: rheological characterization, Colloids Surf. A 201 (2002) 219–230.

[30] Y. Taninouchi, T. Uda, Y. Awakura, Dehydration of CsH_2PO_4 at temperatures higher than 260 °C and the ionic conductivity of liquid product, Solid State Ionics 178 (2008) 1648–1653.

[31] K.J. Zhu, K. Yanagisawa, R. Shimanouchi, Preferential occupancy of metal ions in the hydroxyapatite solid solutions synthesized by hydrothermal method, J. Eur. Ceram. Soc. 26 (2006) 509–513.